Measurement of Viscoelastic Properties of Tissue Mimicking Material Using Longitudinal Wave Excitation

Ali Baghani, *Student Member, IEEE,* Hani Eskandari, *Member, IEEE,* Septimiu Salcudean, *Fellow, IEEE*
Robert Rohling, *Member, IEEE*

***Abstract*— This paper presents an experimental framework for the measurement of the viscoelastic properties of tissue mimicking material. The novelty of the presented framework is in the use of longitudinal wave excitation and the study of the longitudinal wave patterns in finite media for the measurement of the viscoelastic properties. Ultrasound is used to track the longitudinal motions inside a test block. The viscoelastic parameters of the block are then estimated by two methods: a wavelength measurement method and a model fitting method. Connections are also made with shear elastography. The viscoelastic parameters are estimated for a number of homogeneous phantom blocks. The results from the new methods are compared to the conventional rheometry results.**

I. Introduction

The viscoelastic characterization of tissue and tissue mimicking material is of interest in many areas of biomedical research. The variability in tissue stiffness due to anatomical features, as well as the changes incurred in tissue stiffness due to pathology, has led to the development of elastography as a clinical imaging modality [1]–[5]. In general, elastography involves observation of mechanical deformation patterns inside tissue by means of a clinical imaging system and use of these patterns to infer mechanical properties of the tissue being imaged.

To create deformation inside tissue different methods have been devised. Acoustic excitation by sound waves was used by Lerner *et al.* [6], [7]. Ophir *et al.* proposed quasi-static compression [8]. Rudenko *et al.* used acoustic radiation force of focused ultrasound to create shear waves inside tissue [9], [10]. Sandrin *et al.* used external shakers which create longitudinally polarized shear waves [11]–[13]. Excitation by two or more sources of slightly different frequencies has also been considered. The sources are focused ultrasound in the work by Fatemi and Greenleaf [14]. They are shear wave sources in the work by Hoyt *et al.* [15]. Among these works, only Ophir *et al.* used compressional excitation, and only in the quasi-static settings. In all the other cases, either dominantly shear excitation is used, or the compressional excitation is ignored or suppressed by taking the curl of the displacement field.

The authors are with the Department of Electrical and Computer Engineering, University of British Columbia, Vancouver, BC, Canada (e-mail: baghani@ece.ubc.ca).

R. Rohling is co-appointed with the Department of Mechanical Engineering, University of British Columbia, Vancouver, BC, Canada.

To quantitatively study the effectiveness of elastography imaging methods in providing images of viscoelastic properties of tissue, it is of interest to test these methods on phantoms with known anatomical features of known viscoelastic properties. A number of researchers are involved in the development of phantoms with adjustable viscoelastic properties [16]–[23].

Some researchers have used conventional rheometry to validate the results obtained from their elastography techniques [24], [25]. Other researchers have developed specific methods for measuring viscoelastic properties of the phantom and soft tissue specimens [26], [27]. Srinivasan *et al.* used a nanoindenter to measure elasticity [28] . Kalanovic *et al.* compared the results of elasticity measurements with a commercial indenter to the results obtained from their developed shear rheometry device [29]. Egorov *et al.* have developed a soft tissue elastometer which uses a small profile indenter and a scale to measure the applied force [30]. They concluded that the validity of their results depends on the size of the tissue sample relative to the size of the indenter. Samani *et al.* also used a small profile indenter to measure elasticity [31]. FEM was used in their work to study the geometric constant relating the force to the indentation. In their work magnetic resonance imaging based elastography was also proposed for the purpose of rheometry.

Mechanical wave propagation in elastic continua has been studied extensively and is well understood [32], [33]. Some viscoelastic continua have also been studied with certain assumptions about the viscoelastic behavior of the matter [34], [35]. In general the stress-strain relationship for a material can be very complex. The assumption usually made is that the stress-strain relationship can be modeled by linear time invariant differential equations.

Low frequency shear waves were used in the work of Catheline *et al.* for the measurement of the viscoelastic properties of tissue [36]. Longitudinally polarized transient shear waves were produced mechanically and the resulting displacements were tracked by ultrasound speckle tracking to give measurements of the wave speed and attenuation through an inverse problem approach. It was shown that a Voigt model fits the visoelastic behavior of the living tissue better than a Maxwell model.

It is the objective of this research to:

- Show theoretically and experimentally that low frequency longitudinal waves can propagate in a tissue mimicking material of finite dimensions at speeds which are much

lower than those normally associated with ultrasound propagation.
- Show experimentally that it is possible to use ultrasound-based speckle tracking techniques to track the longitudinal waves.
- Show theoretically and experimentally that the measured displacements caused by longitudinal wave propagation can be used to estimate the viscoelastic properties of the tissue mimicking material.

To this end, a new framework is developed for viscoelastic characterization of tissue and phantom specimens by using longitudinal wave excitation and validated against the conventional rheometry.

We start by a brief review of longitudinal wave equations in elastic media in Section II. The experimental setup, material, and methods used are presented in Section III. Section IV is devoted to the presentation of our rheometry methods. The experimental results are presented in Section V and discussed in Section VI. We conclude the paper in Section VII.

II. Theory of wave motion

In this section the theory of wave motion in elastic media is briefly reviewed and the notation used in the article presented. The presentation is adopted from [33]. We start with the model of an elastic medium. We use $\mathbf{u}(\mathbf{x})$ to denote the displacement vector field. τ_{ij} and ϵ_{ij} are used to denote the stress and strain tensors. By definition:

$$\epsilon_{ij} = \frac{1}{2}\left(\frac{\partial}{\partial x_j}u_i + \frac{\partial}{\partial x_i}u_j\right) . \tag{1}$$

The fundamental conservation equations in a medium can then be expressed as:

$$\begin{aligned} \text{mass}: &\quad \tfrac{\partial}{\partial t}\rho + \textstyle\sum_i \tfrac{\partial}{\partial x_i}(\rho \dot{u}_i) = 0 , &(2)\\ \text{momentum}: &\quad \textstyle\sum_j \tfrac{\partial}{\partial x_j}\tau_{ji} + \rho f_i = \rho \ddot{u}_i , &(3)\\ \text{angular momentum}: &\quad \tau_{ij} = \tau_{ji} \quad i \neq j , &(4)\\ \text{energy}: &\quad \rho\dot{e} = \textstyle\sum_{ij} \tau_{ji}\dot{\epsilon}_{ij} . &(5) \end{aligned}$$

where $\rho(\mathbf{x})$ is the density, $\mathbf{f}(\mathbf{x})$ is the force per unit mass vector field, and $e(\mathbf{x})$ is the internal energy per unit mass. These equations hold regardless of the type of the medium. To model the specific behavior of different media, they are concatenated by a set of constitutive equations. These equations model the stress-strain behavior of the medium.

If we assume a homogeneous isotropic elastic medium, under small strains, the constitutive equations widely used are

$$\tau_{ij} = \lambda(\epsilon_{11} + \epsilon_{22} + \epsilon_{33})\delta_{ij} + 2\mu\epsilon_{ij} , \tag{6}$$

where δ_{ij} is equal to one if $i = j$, and zero otherwise. λ and μ are called the Lamé constants.

A number of other constants are also defined based on the Lamé constants,

$$\begin{aligned} E = \mu(3\lambda + 2\mu)/(\lambda + \mu) = \text{Young}'\text{s modulus} , &(7)\\ \nu = \frac{1}{2}\lambda/(\lambda + \mu) = \text{Poisson}'\text{s ratio} , &(8)\\ K = \lambda + \frac{2}{3}\mu = \text{bulk modulus} . &(9) \end{aligned}$$

The inverse of the equation (6) can be expressed in terms of these constants as

$$\epsilon_{ij} = \frac{1+\nu}{E}\tau_{ij} - \frac{\nu}{E}(\tau_{11} + \tau_{22} + \tau_{33})\delta_{ij} . \tag{10}$$

At this point, it is worth defining the scope of our problem in terms of these parameters in dealing with soft human tissue and tissue mimicking material. It has been found experimentally that these materials are nearly incompressible [37], [38]. Hence the Poisson's ratio ν for these materials is very close to 0.5. In this respect, the material under study is closer to liquids such as water and hydraulic oils than to solids such as steel and aluminum. In terms of having a definite shape, a tissue mimicking material is closer to solids than liquids. A number of consequences follow from these peculiar properties:

$$\begin{aligned} \nu &\approx 0.5 , &(11)\\ \lambda &\gg \mu , &(12)\\ E &\approx 3\mu , &(13)\\ K &\approx \lambda . &(14) \end{aligned}$$

In the rest of this article it is assumed that the relations (11) to (14) hold.

The equations (2) to (6) form a complete set of equations for the displacement fields, stresses and density and can be used to derive the most general form of the wave equation [32], [33]. For our purposes it suffices to consider some special cases. We are particularly interested in longitudinal (compressional) waves. The two cases of interest are plane waves in an infinite medium, and plane waves in a finite block of medium.

A. Longitudinal Plane Waves in an Infinite Medium

In this case, it is assumed that particle motion is only in one direction (x_1 direction), i.e. $u_2 = u_3 \equiv 0$. Also because of the symmetry of the plane wave, there is no variation of u_1 in the x_2 and x_3 directions, i.e. $\partial u_1/\partial x_2 = \partial u_1/\partial x_3 \equiv 0$.

These assumptions can be used to derive the wave equation for a longitudinal plane wave propagating in the x_1 direction in an infinite elastic medium,

$$(\lambda + 2\mu)\frac{\partial^2}{\partial x_1^2}u_1 = \rho\frac{\partial^2}{\partial t^2}u_1 . \tag{15}$$

This equation predicts that the wave speed would be

$$c_{\text{inf}} = \sqrt{\frac{\lambda + 2\mu}{\rho}}. \tag{16}$$

Because of the assumptions, in this case the strain tensor takes the form

$$\begin{aligned} \epsilon_{11} &= \frac{\partial}{\partial x_1}u_1 , &(17)\\ \epsilon_{ij} &= 0 \quad \text{otherwise} . &(18) \end{aligned}$$

The stress tensor can be found using the constitutive equations (6),

$$\begin{aligned} \tau_{11} &= (\lambda + 2\mu)\epsilon_{11} , &(19)\\ \tau_{22} &= \lambda\epsilon_{11} , &(20)\\ \tau_{33} &= \lambda\epsilon_{11} , &(21)\\ \tau_{ij} &= 0 \quad \text{otherwise} . &(22) \end{aligned}$$

It is evident from these equations that an infinitesimal cubic volume in the medium experiences normal forces acting on all of its surfaces as the plane wave propagates through that small volume.

Before we move on to the next case, it is important to mention that the wave speed which is widely reported and accepted in the literature for ultrasound is

$$c_{\rm US} = \sqrt{\frac{K}{\rho}} = \sqrt{\frac{\lambda + \frac{2}{3}\mu}{\rho}} \tag{23}$$

where K is the adiabatic compressibility in the case of fluids and bulk modulus in the case of solids [39]. If the tissue is modeled as a fluid and the longitudinal wave propagation as an adiabatic phenomenon, the wave speed would be $c_{\rm US}$. If it is modeled as an elastic solid, the wave speed would be $c_{\rm inf}$ of equation (16). However the difference between these two numbers is much smaller than the accuracy of the practical measurements in this research, so $c_{\rm inf}$ will be used throughout this paper as the ultrasound speed.

Based on ultrasound theory and a large body of evidence, when a small source of longitudinal vibrations (piezoelectric crystal) with sub-millimeter dimensions is placed on the skin, with the human body as the propagation medium, the pulses travel with a speed given by (23) or (16). Therefore for a sub-millimeter wave source of high frequency, the body acts as an infinite medium. As will be shown in the next subsection, the same is not true for all cases of longitudinal wave propagation in solids.

B. Longitudinal Plane Waves in a Finite block of a Medium

Another case of special interest is the propagation of longitudinal waves in material blocks. In this case the effects of finiteness of media should also be taken into account. More specifically, if a *rectangular* block of material is subjected to a spatially uniform, possibly time varying force on one of its surfaces, a longitudinal wave would propagate in the block.

The study of waves of this type could be facilitated by making some assumptions about the stress and strain patterns inside the block. Two main assumptions are made here: that the "strain is uniform on each cross section of the block at every instant", and that "plane sections remain plane under stress". These assumptions make it possible to model the phenomenon as a one-dimensional problem.

We further elaborate on these assumptions. A medium with a finite cross section acts as a waveguide for elastic waves. At each frequency of excitation a number of spatial modes are excited. Each of these modes has its own wave speed associated with it. As a result the wave speed depends on the frequency of excitation. Now consider an infinitely long rod of finite cross section which experiences a spatially uniform low frequency compression over its cross section. Under these conditions the dominant mode of the rod has a wave pattern which satisfies the assumptions made here [32]. More precisely, at low frequencies only the first mode is excited and the amplitude of vibrations is almost constant over the cross section. This justifies the use of the assumptions made here and the use of a 1D model.

Now assume that the wave is propagating in the x_1 direction. The fact that the block has free boundaries on its sides causes the lateral stresses to vanish on the surfaces,

$$\tau_{22} = 0\,, \tag{24}$$
$$\tau_{33} = 0\,, \tag{25}$$
$$\tau_{ij} = 0 \quad i \neq j\,. \tag{26}$$

Because of the assumptions made, these conditions hold throughout the block. If not, the infinitesimal volumes located around the boundary of the block, would be (axially) compressed more, because of the absence of lateral stresses, than internally located infinitesimal volumes. As a result plane sections would not remain plane anymore which contradicts the assumptions. Moreover, the top and bottom boundaries of the block should be frictionless slip boundaries to prevent any external lateral forces on them.

Now the constitutive equation (10) gives

$$\begin{aligned} \epsilon_{11} &= \frac{1+\nu}{E}\tau_{11} - \frac{\nu}{E}\tau_{11} \\ &= \frac{1}{E}\tau_{11}\,, \end{aligned} \tag{27}$$

or equivalently

$$\begin{aligned} \tau_{11} &= E\epsilon_{11} \\ &= \frac{\mu(3\lambda+2\mu)}{\lambda+\mu}\epsilon_{11}\,. \end{aligned} \tag{28}$$

As a result, the equation of a longitudinal wave propagating in the x_1 direction in the block would be

$$\frac{\mu(3\lambda+2\mu)}{\lambda+\mu}\frac{\partial^2}{\partial x_1^2}u_1 = \rho\frac{\partial^2}{\partial t^2}u_1\,. \tag{29}$$

This equation predicts that longitudinal waves propagate in the block at a speed of

$$c_{\rm fin} = \sqrt{\frac{\frac{\mu(3\lambda+2\mu)}{\lambda+\mu}}{\rho}} = \sqrt{\frac{E}{\rho}}\,. \tag{30}$$

A comparison of (30) with (16) shows that the propagation speed of longitudinal (compressional) waves is different in finite blocks as compared to infinite media of the same material. For nearly incompressible material $c_{\rm fin} \approx \sqrt{3\mu/\rho} = \sqrt{3}c_S$ where $c_S = \sqrt{\mu/\rho}$ is the shear wave speed in the infinite medium. This speed is in the order of 1 to 10m/s for soft tissue which is much smaller than $c_{\rm inf}$ which is approximately 1540m/s.

Since $c_{\rm fin}$ is much smaller than $c_{\rm inf}$, it is possible to track the longitudinal wave propagation in blocks of tissue using pulsed ultrasound. Our objective is to perform rheometry measurements by studying the longitudinal wave patterns inside finite blocks of tissue phantoms. In the next section the apparatus and methods used to create these wave patterns and collect data are presented. The proposed rheometry methods for analyzing the collected data follow in Section IV.

III. Experimental Methods and Setup

In this section the experimental setup is discussed, and the acquired data are described. For ultrasound elastography studies, a device has been developed which is capable of applying dynamic compressions to a phantom while it is being imaged by an ultrasound probe. The detailed description of this device can be found in [40].

Figure 1 shows a simplified schematic of this device. The device has two plates between which the phantom is compressed. The upper plate is connected to the chassis and does not move. This plate has an opening for an ultrasound probe, and fitted by a linear array ultrasound probe. The lower plate is confined to move in one direction by a linear bearing. This plate is connected to a cam follower mechanism sitting on a cam driven by a controlled DC motor.

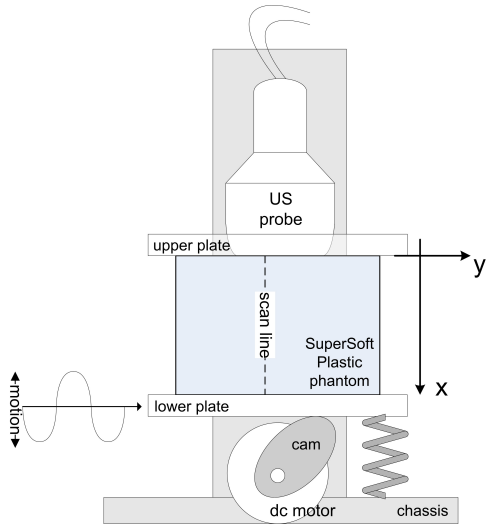

Fig. 1. Simple schematic of the rheometry device

For testing, a rectangular phantom block is placed between the two plates and the height of the upper plate is adjusted to have some pre-compression on the phantom to ensure contact with the ultrasound transducer is maintained. By (24) - (26) it is required that the top and bottom surfaces of the block only experience forces in the vertical direction. To match the experimental conditions to the theoretical ones, ultrasound gel was used as a lubricant on the top and bottom surfaces of the phantom in contact with the plates to reduce the friction.

Super Soft Plastic™ (M-F Manufactureing Co., Inc. Fort Worth, Tx, USA), a PVC (Poly Vinyl Chloride) based plastic, was used as the phantom material. The stiffness of this material can be adjusted by adding Plastic Softener™ or Plastic Hardener™ provided by the same company. SigmaCell® Cellulose, Type 50 (Sigma-Aldrich Inc., St Louis, MO, USA) was added to the phantoms as the ultrasound scatterer to develop the speckle pattern needed for ultrasound-based motion tracking. For each 100mL of liquid plastic, 1mL of cellulose was added. We used a 40mm×30mm×30mm mold to fabricate five homogeneous blocks with different stiffnesses. The fabrication parameters, together with the measured densities and ultrasound speeds $c_{\inf}$ for these phantoms are summarized in Table I. The densities were measured by weighing the phantoms with a precision scale, and measuring the block dimensions with calipers and dividing the mass by the calculated volume. The ultrasound speed was found by first measuring the depth to the bottom of the phantom on a B-mode ultrasound image which is displayed on the ultrasound machine assuming an ultrasound speed of 1540m/s, and then correcting the speed so that the measured depth matches the height of the phantom. As can be seen, the density and $c_{\inf}$ are not greatly affected by changing the proportion of Plastic to Softener or Hardener.

TABLE I

Fabrication and measured properties of the five test phantoms

phantom No	Plastic (volume portion)	Hardener (volume portion)	Softener (volume portion)	density (kg/m^3) $\pm 5\%$	ultrasound speed (m/s)$\pm 1\%$
1	4	0	2	1020	1420
2	5	0	1	1030	1420
3	6	0	0	990	1410
4	5	1	0	1010	1440
5	4	2	0	1030	1410

TABLE II

Parameters of the ultrasound imaging system

parameter	value
probe type	L9–4 linear array
center frequency	4MHz
sampling frequency	20MHz
depth of focus	25mm
imaging depth	40mm
Doppler pulse repetition frequency	2.5kHz
number of samples acquired	75,472

In all the experiments the lower plate was excited with Gaussian white-noise, band-limited to 4–150Hz, while RF-lines were collected for 30 seconds at a rate of 2500 lines/second in the Doppler mode from a single A-line. The imaging system used was a Sonix RP ultrasound machine (Ultrasonix Medical Corp., Richmond, BC, Canada). The parameters of the imaging system are summarized in Table II.

The acquired RF-line data were processed off-line to obtain the displacement profile of each point along the scan line. Since the models used are 1D models, only the axial displacements were calculated. Lateral displacements also occur which could be used to improve the estimations in future work. The algorithm used for displacement calculations is described in [41]. The parameters used are summarized in Table III. We use the notation $u_{\mathrm{m}}(x,t)$ to denote the measured displacement of a point located at depth x at time t. It is worth mentioning that both x and t are discrete variables in this notation.

The discrete Fourier transform was then applied to $u_{\mathrm{m}}(x,t)$ to obtain the *phasor* displacement profile $U_{\mathrm{m}}(x,j\omega)$. Frequency domain averaging was also used, as provided by the `tfestimate` function of MATLAB® to smooth the data. The data were normalized at each frequency separately so that the element located at $x = 40\mathrm{mm}$ would have unit amplitude and zero phase. This normalization does not have any effect on the results, but it helps with the plotting of the phasor data.

At each frequency ω, $U_{\mathrm{m}}(x,j\omega)$ is a complex-valued func-

TABLE III
PARAMETERS OF THE SPECKLE TRACKING MOTION ESTIMATION ALGORITHM

parameter	value
number of blocks	80
block length	1mm
block overlap	50%
displacement measurement	relative (corresponding to block velocity)
stretching	not used

tion of x which gives the steady-state displacement phasor of a point located at x inside the phantom, if the phantom were excited with frequency ω. A typical phasor profile is plotted in Fig. 2. Parts (a) and (b) show the amplitude and phase of the phasor profile as a function of depth x, while part (c) shows the same profile as a curve in the complex plane (parameterized by the depth x). In the next section $U_{\rm m}(x, j\omega)$ will be used to characterize the viscoelastic properties of the phantoms.

To validate our estimation results, we collected conventional rheometry data from the phantoms. This was achieved by a modification to the device of Fig. 1, where the ultrasound probe and upper plate were replaced by a force sensor (Load Cell MDB-2.5, Transducer Techniques, Temecula, CA, USA). The rheometry device was reported in a previous article [40]. More details about the rheometry method used in this article can be found in the Appendix.

IV. PROPOSED RHEOMETRY METHODS

In this section two methods are introduced for analyzing the obtained data presented in the previous section for estimation of viscoelastic properties of tissue phantoms. We start by deriving a viscoelastic model for the phantom block to be used in these methods.

Longitudinal wave propagation in a viscoelastic block can be modeled in a number of different ways [32], [33]. The most complete model is obtained by solving the three dimensional wave equation in a viscoelastic medium with boundary conditions adopted to match that of the block. Except for some special cases for which analytical solutions have been derived [33], this model is quite difficult to solve and requires numerical methods such as finite element methods. Thus approximate models are usually used.

The simplest approximate model is the model presented in equation (29) of subsection II-B. From now on for brevity we denote the first coordinate by $x \equiv x_1$. In the frequency domain, this equation becomes

$$\begin{aligned}(j\omega)^2\rho U &= \frac{\mu(3\lambda+2\mu)}{\lambda+\mu}\frac{\partial^2}{\partial x^2}U \\ &= E\frac{\partial^2}{\partial x^2}U. \end{aligned} \quad (31)$$

A next step in the modeling is the introduction of a first order viscosity term. The Voigt model was shown to more closely follow the behavior of the soft tissue [36]. In this case

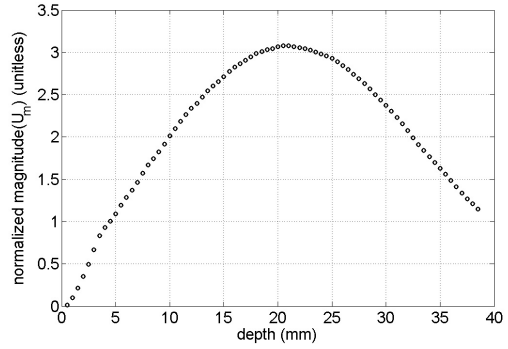

(a)

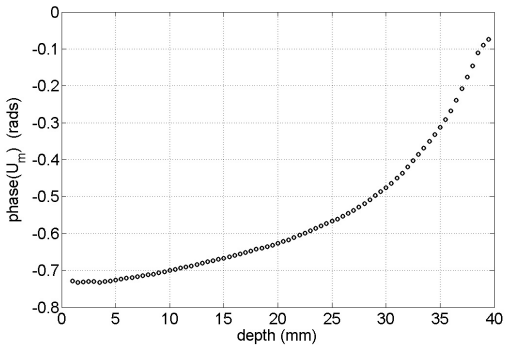

(b)

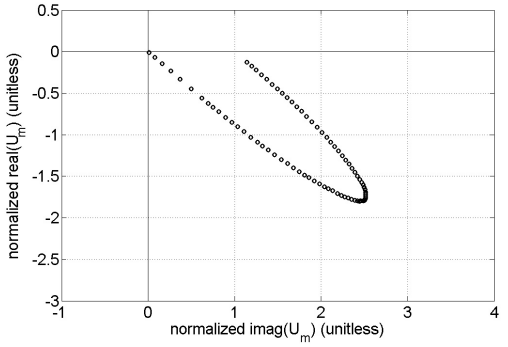

(c)

Fig. 2. A typical normalized displacement phasor profile, belonging to phantom No.3 at a frequency of 90Hz. The (a) magnitude and (b) phase of the phasor profile (c) the same normalized phasor profile in the complex plane. The profile is normalized to the phasor of the point at $x = 40\text{mm}$.

the wave equation becomes

$$\begin{aligned}(j\omega)^2\rho U &= E\frac{\partial^2}{\partial x^2}U \\ &\quad + Bj\omega\frac{\partial^2}{\partial x^2}U, \end{aligned} \quad (32)$$

where B models first order viscosity effects. This is basically equivalent to assuming a Voigt model for the stress-strain relation of the material. The ratio B/E is called the *relaxation time*.

Note that both of the equations (31) and (32) have the form

$$(j\omega)^2 U = c_{\rm fin}^2(\omega)\frac{\partial^2}{\partial x^2}U\,, \quad (33)$$

where $c_{\rm fin}(\omega)$ is a complex frequency-dependent wave speed given by,

$$c^2_{\rm fin}(\omega) = \begin{cases} \dfrac{E}{\rho}, & \text{for (31)} \\ \dfrac{E}{\rho} + j\dfrac{B\omega}{\rho}, & \text{for (32)} \end{cases} . \quad (34)$$

The steady state solution to (33) can be found easily. Consider the characteristic equation of this differential equation,

$$s^2 + \frac{\omega^2}{c^2_{\rm fin}(\omega)} = 0\,, \quad (35)$$

and denote its roots by $s_1(\omega) = -s_2(\omega) = \alpha(\omega) + j\beta(\omega)$. Then, the steady state solution to (33) is of the form:

$$\begin{aligned} U(x, j\omega; E, B) \quad &= A_1 \exp\left((\alpha(E,B) + j\beta(E,B))x\right) \\ &\quad + A_2 \exp\left((-\alpha(E,B) - j\beta(E,B))x\right), \end{aligned} \quad (36)$$

where A_1 and A_2 are determined by boundary conditions.

In our experimental setup (Fig. 1), the sample is confined at $x = 0$, i.e. $u(0,t) \equiv 0$, as a result

$$U(0, j\omega) \equiv 0 = A_1 + A_2\,, \quad (37)$$

and therefore $A_2 = -A_1$. The phasor solution (36) in this case could be simplified to obtain,

$$\begin{aligned} U(x, j\omega) \quad &= \quad 2A_1 \left(\cos(\beta x)\sinh(\alpha x)\right. \\ &\quad \left. + j\sin(\beta x)\cosh(\alpha x)\right)\,, \end{aligned} \quad (38)$$

where A_1 is determined by the amplitude of the excitation at x =40mm. This solution is similar to a standing wave solution. However in a standing wave solution all the points have the same phase, whereas in equation (38) different spatial points have different phases. If the viscosity is negligible ($\alpha = 0$) standing waves are produced.

In the following subsections, the derived models will be used to propose two methods for the estimation of the viscoelastic parameters of the phantom blocks.

A. Peak to Node Method

This method can be used to estimate Young's modulus for a block of material, based on the longitudinal wave pattern observed inside the block. From (38) the amplitude of the solution, after some manipulation, can be found as

$$|U(x, j\omega)|^2 = 4A_1^2\left(\sinh^2(\alpha x) + \sin^2(\beta x)\right)\,. \quad (39)$$

Now if the viscosity is small, the model (31) can be used and the solution to the characteristic equation (35) would be

$$\alpha + j\beta = j\frac{\omega}{\sqrt{\frac{E}{\rho}}}\,, \quad (40)$$

or,

$$\begin{aligned} \alpha \quad &= \quad 0\,, & (41) \\ \beta \quad &= \quad \frac{\omega}{\sqrt{\frac{E}{\rho}}}\,. & (42) \end{aligned}$$

In this case, (39) becomes

$$|U(x, j\omega)| = 2A_1\left|\sin\left(\frac{\omega}{\sqrt{\frac{E}{\rho}}}x\right)\right|\,. \quad (43)$$

The distance of a node to a peak, $d_{\rm np}$, of the wave pattern is equal to a quarter of the wavelength, therefore

$$\begin{aligned} c_{\rm fin} \quad &= \quad (4\,d_{\rm np})\frac{\omega}{2\pi}\,, & (44) \\ E \quad &= \quad \rho c^2_{\rm fin}\,. & (45) \end{aligned}$$

In our case the node is at x =0mm and at each frequency, the peak is found by searching for a local maximum in a filtered version of the amplitude of $U_m(x, j\omega)$.

In summary, the peak to node method estimates Young's modulus based on the peak to node distance of a measured phasor profile $U_m(x, j\omega)$ using equation (45). But this method does not provide estimates of viscosity or relaxation time. In the next subsection another method is presented which also estimates the viscosity.

B. Model Fitting Method

A more general method to characterize the viscoelastic properties of the sample block is to use the characteristic equation (35) to determine the complex wave speed, $c_{\rm fin}(\omega)$, for different excitation frequencies, ω, experimentally, and then use a parameterization of the viscoelastic properties, such as that presented in (34) to find the particular parameters of interest.

Alternatively, one of the parameterized models (34) can be directly fitted to the data. We present this approach here. The viscoelastic model was chosen and the general solution (36) was fitted to the data by least squares optimization over the parameters A_1, A_2, E and B. Thus for each frequency the following cost function was minimized:

$$J(\omega) = \sum_x \left|U_m(x, j\omega) - U_m(x, j\omega; E, B)\right|^2\,. \quad (46)$$

Figure 3 shows a typical fitted model. As can be seen the model fits the data very well. In the next section the normalized mean squared error (NMSE) is used to quantitatively ensure that the model fits the data well.

V. Results

The proposed rheometry methods of Section IV were applied to the data collected using the apparatus and methods of Section III. The results for the five phantoms follow in this section.

A. Peak to Node Results

The peak to node method was used to analyze the measured phasor profiles $U_{\rm m}(x, j\omega)$ for the five phantom blocks. Note that (44) and (45) could be calculated at any frequency for which there is a node and a peak present in the phasor profile (see Fig. 2 (a)). As a result, this method cannot be used at very low frequencies, since no peaks occur within the 40mm height of the phantom. Figure 4 shows the estimated $c_{\rm fin}(\omega)$ for the

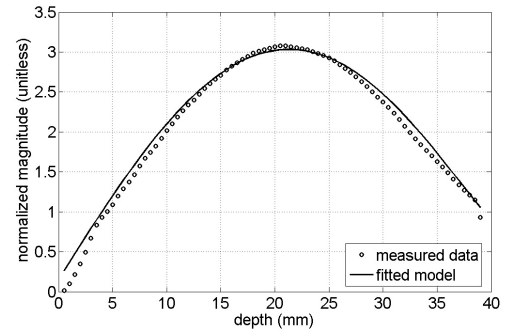

(a)

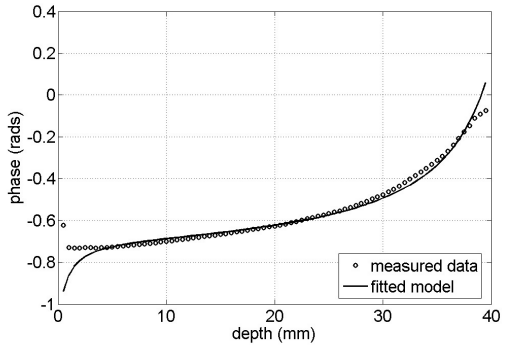

(b)

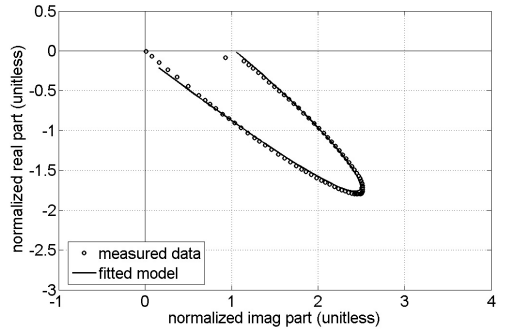

(c)

Fig. 3. Fitted model to the measured displacement data. The data is the same as that of Fig. 2, which is from phantom No. 3 at 90Hz. (a) absolute value and (b) phase of the phasor profile (c) the same normalized phasor profile in the complex plane.

test phantom No. 3 over the range of frequencies where this method could be used. The average speed over this frequency range, $c_{\rm fin}$, is equal to 7.5m/s and the standard deviation is equal to 0.29m/s. The Young's modulus calculated based on this average speed is 55kPa.

The same method was used to estimate longitudinal wave speed and Young's modulus for the other four test phantoms. The results are summarized in Table IV. Also presented are the values obtained from conventional rheometry on the same blocks. As can be seen the results are generally in good agreement and this supports the validity of the model and thus the assumptions.

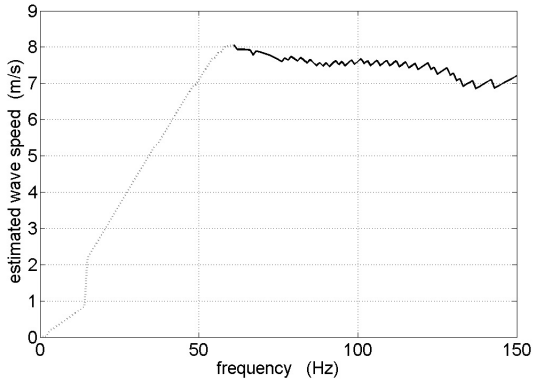

Fig. 4. Estimated $c_{\rm fin}(\omega)$ for phantom No.3. Plotted in dark solid line is the selected region for estimation of average speed. At lower frequencies no peak occurs inside the block length.

TABLE IV

ESTIMATED VALUES OF LONGITUDINAL WAVE SPEED $c_{\rm fin}$ AND YOUNG'S MODULUS FOR THE TEST PHANTOMS USING THE PEAK TO NODE METHOD

phantom No	average wave speed ±std (m/s)	freq. range used (Hz)	peak to node Young's modulus ±std (kPa)	conventional rheometry Young's modulus±10% (kPa)	error
1	4.4±0.15	30–90	19±1.5	21	11%
2	5.2±0.25	40–110	28±2.1	32	11%
3	7.5±0.29	60–150	55±4.6	56	2%
4	8.7±0.27	70–150	76±6.0	76	0%
5	12 ±0.13	90–150	140±13	127	10%

B. Model Fitting Results

The model fitting approach was used to find the values of Young's Modulus E and relaxation time for the five phantom blocks. Figure 5 compares the results to the conventional rheometry results. In Fig. 5(a) the model-fitting and rheometry values of the Young's modulus, E, for different frequencies are plotted. The model fitting plots are limited to frequencies for which the normalized mean squared error defined by

$$\text{NMSE} = \sqrt{\frac{J(\omega)}{\sum_x \left|U_m(x,j\omega) - \text{mean}\left(U_m(x,j\omega)\right)\right|^2}}, \quad (47)$$

is better than 10%. This threshold was used to ensure that the model fitted the data well enough for further conclusions to be valid. The rheometry plots are limited to 40Hz. As expected, the values of E from model fitting matches with rheometry values. The average values and standard deviations are summarized in Table V.

In Fig. 5(b) the optimized values of the relaxation times together with the values obtained from the conventional rheometry are presented. Note that both axes are in logarithmic scale in this figure. Again the data of the conventional rheometry are limited to 40Hz. As can be seen from this figure, the general trends and values of relaxation times from model fitting match that of conventional rheometry. Also a power-law decrease in the relaxation time with the increase of the frequency is observed which is consistent with the previous reports [40].

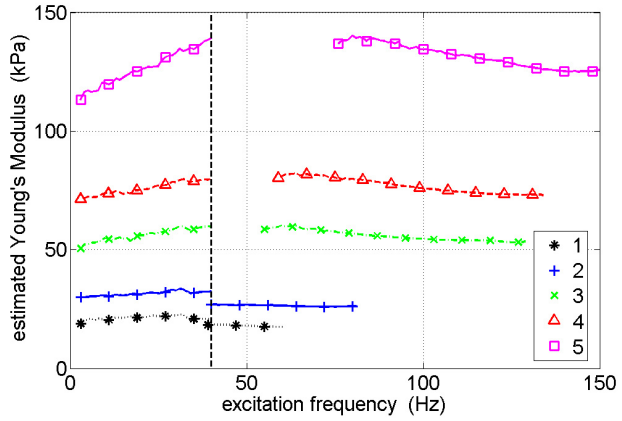

(a)

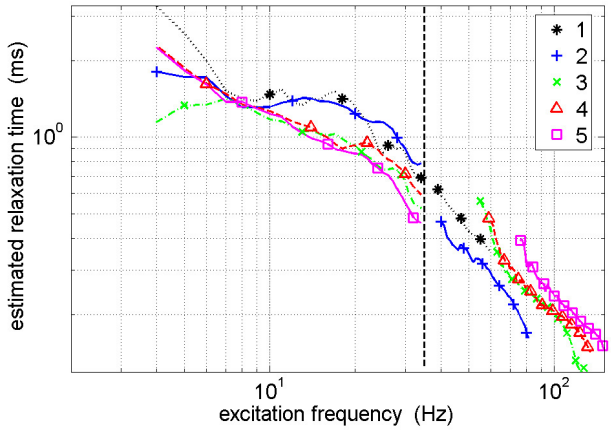

(b)

Fig. 5. (a) Estimated value of the Young's modulus and (b) relaxation times for the five phantoms at different frequencies of excitation. The lower frequency graphs (4–40Hz) are from conventional rheometry and the higher frequency graphs (above 40Hz) are from model fitting.

TABLE V

ESTIMATED VALUES OF LONGITUDINAL WAVE SPEED c_{fin} AND YOUNG'S MODULUS FOR THE TEST PHANTOMS USING THE MODEL FITTING METHOD

phantom No	wave speed ±std (m/s)	freq. range used (Hz)	model fitting Young's modulus ±std (kPa)	conventional rheometry Young's modulus±10% (kPa)	error
1	4.2±0.15	50–60	18±1.3	21	16%
2	5.0±0.18	40–80	26±1.9	32	18%
3	7.4±0.29	55–130	55±4.4	56	2 %
4	8.7±0.34	60–135	77±6.1	76	1 %
5	11.3±0.46	75–150	132±11	127	4 %

VI. DISCUSSION

It has been shown experimentally by Catheline *et al.* [36] that when a finite block of viscoelastic material is vibrated by a compressional exciter with a *small* cross sectional area, two waves propagate in the block: a compressional wave which parts almost instantaneously at the speed of ultrasound, *i.e.* 1540m/s, and a longitudinally polarized slow shear wave, which follows with the shear wave speed, *i.e.* $\sqrt{\mu/\rho}$ which is around 1-10m/s. The shear wave can be tracked by ultrasound speckle tracking and the displacements can be used to measure the viscoelastic properties of the block.

We have shown here that when a finite block of viscoelastic material is vibrated by a compressional exciter with a *large* cross sectional area which covers the entire top surface of the block, instead of the longitudinally polarized slow shear wave, a slow longitudinal wave propagates with the speed $c_{\text{fin}} = \sqrt{E/\rho} \approx \sqrt{3\mu/\rho}$ which is around 5-15m/s. This longitudinal wave can also be tracked by ultrasound speckle tracking and the displacements can be used to measure the viscoelastic properties of the block.

To show how the size of the exciter affects the wave speed we conducted two different experiments with the same phantom block, namely block No. 1, similar to the experiments of [36]. In the first experiment, a plate exciter was used which covered the entire top surface of the phantom. The surface was lubricated with ultrasound gel to minimize the friction between the plate and the phantom. A single period of 50Hz sinusoid was used as a transient excitation. The exciter was an open loop voice coil. Therefore the actual mechanical vibration transferred to the phantom was not exactly a single period of 50Hz, but had some tail. One scan line (A-line) was sampled at 5kHz and the displacements tracked. The displacements at different depths are plotted as a function of time in Fig. 6(a). By looking at the wave front the speed is approximately 3.7m/s. This speed is $\sqrt{3\mu/\rho}$ which was also reported in Tables IV and V. The slight difference is due to a few months time interval between the conduction of the experiments. The properties of the phantom have shifted slightly over time.

The same phantom was used for a second experiment. This time, instead of the plate, a small screw was connected to the voice coil, which acted almost like a point source. The result for this case is presented in Fig. 6(b). The speed from this figure is approximately 2.3m/s. This is the wave speed Catheline *et al.* reported in [36], *i.e.* the shear wave speed $\sqrt{\mu/\rho}$.

Note that in both cases Fig. 6(a) and (b), just after the compression is applied, a compressional wave front is generated which propagates through the phantom at the speed of ultrasound, *i.e.* 1420m/s. The initial propagation of this wave front cannot be tracked by the ultrasound, since the speed of ultrasound is the same as the wave speed. This wave front probes the boundaries of the medium and gets reflected back. However the displacements caused by multiple reflections of this wave from the boundaries are present in the phantom. The displacements, as shown by Sandrin *et al.* [13], are very small and can barely be detected by our speckle tracking algorithm.

Super Soft Plastic$^{\text{TM}}$ was shown to be a promising phantom

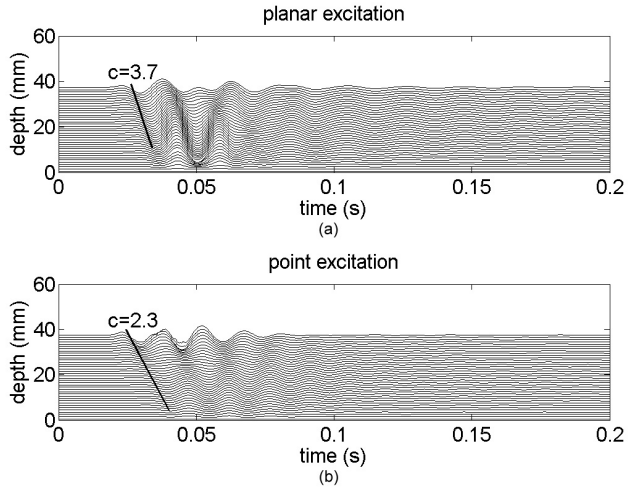

Fig. 6. (a) The result of the excitation with a plate which covers the top surface of the phantom (b) The result of the excitation with a point source.

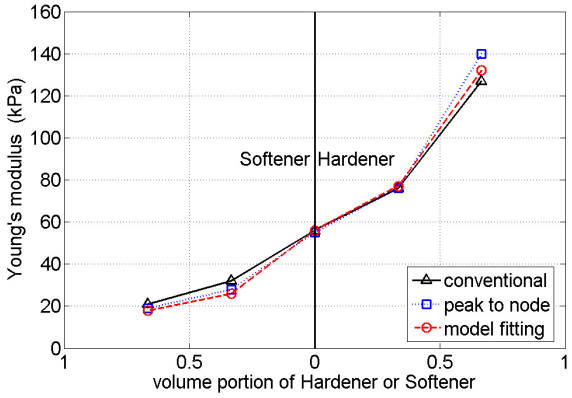

Fig. 7. Obtained Young's modulus as a function of the volume portion of Plastic Softener or Hardener added during the fabrication of the phantoms

material for elastography studies, as its Young's (and hence shear) modulus can be adjusted over a wide range (15–150kPa), without changing its density and the speed of ultrasound $c_{\inf}$ (Table I). Figure 7 summarizes the Young's modulus obtained vs. the volume portion of hardener or softener used in the fabrication process for this material. However, the relaxation time and its frequency dependent behavior is not dependent on the volume portion of Softener or Hardener, as the graphs in Fig. 5(b) almost overlap for the five test blocks. Therefore without any additives, this material by itself is unsuitable for creating phantoms with significant viscosity contrast.

In the previous sections, measurement results for $c_{\inf}$ (ultrasound speed) and E were presented. If a purely elastic medium is assumed, these measurements can be used to obtain all the elastic parameters. Other elastic parameters, namely Lamé constants λ and μ, and Poisson's ratio ν could be easily found using the relations (7) to (9). The parameters are summarized in Table VI for the five phantoms. The values of the Young's modulus from the model fitting method were used in the calculations.

TABLE VI

SUMMARY OF THE ELASTIC PROPERTIES OF THE FIVE TEST PHANTOMS

phantom No	λ (GPa)	μ (kPa)	E (kPa)	0.5 - ν 1E-6$\times$	K (GPa)
1	2.1	6.0	18	1.5	2.1
2	2.1	8.7	26	2.1	2.1
3	2.0	18	55	4.7	2.0
4	2.1	26	77	6.1	2.1
5	2.0	44	132	11	2.0

The speed of ultrasound $c_{\inf}$ has little variability among different soft tissue types which are usually scanned using ultrasound imaging systems. This fact allows the conversion of time scale of ultrasound RF-pulses to distance for ultrasound image formation. This was also true for the Super Soft Plastic$^{\text{TM}}$ used in our experiments. This fact has another important consequence which has been noted by other scholars as well [3]. Since soft tissue is nearly incompressible, $\lambda \gg \mu$; hence $c_{\inf}$ is determined mainly by λ. In other words μ has no contribution. Since the variability of density is also very low (in living tissue and phantoms), λ should be almost constant. As a result, the first Lamé constant, λ, is not an elastic parameter of interest for creating contrast in elastograms. In contrast, tissue stiffness is determined by Young's modulus, E, which for incompressible materials is equal to 3μ, and a great variability exists here. As a result, the second Lamé constant, μ, (or Young's modulus, E) is the parameter of interest in elastography.

From this discussion, a connection can be made between elastography methods based on shear wave excitation and methods based on longitudinal wave excitation. In shear wave excitation, shear wave speed $c_S = \sqrt{\mu/\rho}$ and hence shear modulus, μ is sought. In longitudinal excitation, Young's modulus $E = 3\mu$ is sought. Hence these methods, although different in many aspects, essentially use the same underlying physical quantity to create elastogram contrast.

Another important point is that at low frequencies of excitation the phase difference in oscillations of the different points is low because of the large wavelength. Hence it is more difficult if not impossible to estimate the viscoelastic properties by using a low frequency. We conclude that a lower limit for the frequency of excitation exists. Note that this statement only applies to the estimation of the *absolute values* of the viscoelastic properties using the wave equation; *relative* estimations are still possible though. As a matter of fact, for a static compression $\partial u/\partial t \equiv \partial^2 u/\partial t^2 \equiv 0$. In this case the wave equation (29) implies $\partial^2 u/\partial z^2 \equiv 0$. The wave equation itself will become,

$$\rho \times 0 = E \times 0\,, \tag{48}$$

which cannot be inverted. However the strain, which is given by $\epsilon = \partial u/\partial z$ is not necessarily equal to zero. Assuming a uniform stress, the strain is inversely proportional to the Young's modulus E, and hence relative values of E can be obtained from the relative values of ϵ. If in addition, force measurement is carried out, the relative values can be turned into absolute values.

It was observed that one-dimensional models would not

fit the data very well at higher frequencies of excitation. It is known that a block of material acts as a wave-guide for elastic wave propagation [32], and the wave speed depends on the dimensions of the source (the excited modes of the wave guide) as well as the frequency of excitation. Further study of these effects is needed.

Finally, the assumption of a 1D model which was made for the displacements is a limiting assumption. However, the methods presented in this article are intended for rheometry purposes, i.e. characterization of the viscoelastic behavior of a test block assuming homogeneity. The traditional force-displacement rheometry methods treat the entire test block as one unit, while in the presented methods an insight into internal vibrations inside the block is obtained as well. Moreover no force measurements are carried out. The presented methods do not yield local viscoelastic properties and hence are not presented as an alternative to any of the techniques intended for that purpose. Many research groups are looking at this problem, *i.e.* solving the inverse problem, from different perspectives. In particular they use a more complete model, such as a 2D or 3D model, for the local inversion. This article, however, shows that longitudinal waves can also be a valid candidate for forming elastograms and extending the inverse problem methods to this type of excitation.

VII. Summary and Conclusion

In this article an experimental framework was presented for viscoelastic characterization of tissue and tissue mimicking material. Longitudinal wave excitation was used on five blocks of test phantoms and displacements were imaged by an ultrasound system. Two methods were presented for analyzing the displacements. The first method estimated the Young's modulus based on the distance from the peak to the node of the standing wave patterns inside the block. The second method used a model fitting scheme to find the values of the Young's modulus and the relaxation time. The results were compared to conventional rheometry results obtained using force-displacement measurements. For the elasticities good agreement was observed which validated the theory. For the viscosities, only the trends could be compared as the measurements were over different frequency ranges.

We conclude that the speed of the longitudinal waves in finite media can be orders of magnitude lower than their speed in infinite media and in fact comparable to the speed of shear waves. It is possible to track these waves by using the ultrasound-based motion tracking techniques. The longitudinal waves cannot simply be dismissed because of their presumed high speed of propagation or their insignificant amplitude. The viscoelastic properties of homogeneous phantom blocks can be estimated by applying the methods presented in this article on the longitudinal displacements. The methods are based on fitting a longitudinal-wave-equation-based model to the measured displacements. The estimated properties would be in agreement with the gold standard values from the conventional rheometry tests. Whether the human body or a particular tissue sample *in vivo* or *ex vivo* can be regarded as a finite medium, however, depends on the geometry of the setup and the excitation used and needs further analysis.

Acknowledgment

This research was supported by the Natural Sciences and Engineering Research Council (NSERC) of Canada. The authors would like to thank Reza Zahiri-Azar for the speckle tracking software.

References

[1] A. Sarvazyan, "Handbook of elastic properties of solids, liquids and gases," vol. III, 2001.

[2] K. Parker, L. Gao, R. Lerner, and S. Levinson, "Techniques for elastic imaging: A review," *IEEE Eng. Med. Biol. Mag.*, vol. 15, no. 6, pp. 52–59, 1996.

[3] J. F. Greenleaf, M. Fatemi, and M. Insana, "Selected methods for imaging elastic properties of biological tissues," *Annu. Rev. Biomed. Eng.*, vol. 5, pp. 57–78, April 2003.

[4] K. J. Parker, L. S. Taylor, S. Gracewski, and D. J. Rubens, "A unified view of imaging the elastic properties of tissue," *J. Acoust. Soc. Am.*, vol. 117, no. 5, pp. 2705–2712, May 2005.

[5] J. Ophir, S. K. Alam, B. Garra, F. Kallel, E. Konofagou, T. Krouskop, C. Merritt, R. Righetti, R. Souchon, S. Srinivasan, and T. Varghese, "Elastography: Imaging the elastic properties of soft tissues with ultrasound," *Journal of Medical Ultrasonics*, vol. 29, pp. 155–171, 2002.

[6] R. Lerner and K. Parker, "Sonoelasticity images, ultrasonic tissue characterization and echographic imaging," in *Proceedings of the 7th European Communities Workshop*, 1987, nijmegen, Netherlands.

[7] R. Lerner, K. Parker, J. Holen, R. Gramiak, and R. Waag, "Sono-elasticity: Medical elasticity images derived from ultrasound signals in mechanically vibrated targets," *Acoustical Imaging*, vol. 16, pp. 317–327, 1988.

[8] J. Ophir, I. Cespedes, H. Ponnekanti, Y. Yazdi, and X. Li, "Elastography: A quantitative method for imaging of elasticity of biological tissues," *Ultrason. Imaging*, vol. 13, pp. 11–134, 1991.

[9] O. Rudenko, A. Sarvazyan, and S. Emelianov, "Acoustic radiation force and streaming induced by focused nonlinear ultrasound in a dissipative medium," *J. Acoust. Soc. Am.*, vol. 99, no. 5, pp. 2791–2798, May 1996.

[10] A. Sarvazyan, O. Rudenko, S. Swanson, J. Fowlkes, and S. Emelianov, "Shear wave elasticity imaging: A new ultrasonic technology of medical diagnostics," *Ultrasound Med. Biol.*, vol. 24, no. 9, pp. 1419–1435, 1998.

[11] L. Sandrin, M. Tanter, J.-L. Gennisson, S. Catheline, and M. Fink, "Shear elasticity probe for soft tissue with 1-d transient elastography," *IEEE Trans. Ultrason., Ferroelect., Freq. Contr.*, vol. 49, no. 4, pp. 436–446, April 2002.

[12] L. Sandrin, M. Tanter, S. Catheline, and M. Fink, "Shear modulus imaging with 2-d transient elastography," *IEEE Trans. Ultrason., Ferroelect., Freq. Contr.*, vol. 49, no. 2, pp. 426–435, April 2002.

[13] L. Sandrin, D. Cassereau, and M. Fink, "The role of the coupling term in transient elastography," *J. Acoust. Soc. Am.*, vol. 115, no. 1, pp. 73–83, January 2004.

[14] M. Fatemi and J. Greenleaf, "Ultrasound stimulated vibro-acoustic spectrography," *Science*, vol. 280, pp. 82–85, 1998.

[15] K. Hoyt, K. J. Parker, and D. J. Rubens, "Real-time shear velocity imaging using sonoelastographic techniques," *Ultrasound Med. Biol.*, vol. 33, no. 7, pp. 1086–1097, 2007.

[16] B. Chan, J. V. Merton-Gaythrope, M. P. Kadaba, S. Zafaranloo, and D. Bryk, "Acoustic properties of polyvinyl chloride gelatin for use in ultrasonography," *Radiology*, pp. 215–216, 1984.

[17] T. J. Hall, M. Bilgen, M. F. Insana, and T. A. Krouskop, "Phantom materials for elastography," *IEEE Trans. Ultrason., Ferroelect., Freq. Contr.*, vol. 44, no. 6, pp. 1355–1365, 1997.

[18] C. M. Hassan and N. A. Peppas, "Structure and applications of poly(vinyl alcohol) hydrogels produced by conventional crosslinking or by freezing/thawing methods," *Advances in Polymer Science*, vol. 153, pp. 37–65, 2000.

[19] E. Madsen, G. Frank, T. Krouskop, T. Varghese, F. Kallel, and J. Ophir, "Tissue-mimicking oil-in-gelatin dispersions for use in heterogeneous elastography phantoms," *Ultrasonic Imaging*, vol. 25, pp. 17–38, 2003.

[20] E. L. Madsen, M. A. Hobson, G. R. Frank, H. Shi, J. Jiang, T. J. Hall, T. Varghese, M. M. Doyley, and J. B. Weaver, "Anthropomorphic breast phantoms for testing elastography systems," *Ultrasound Med. Biol.*, vol. 32, no. 6, pp. 857–874, 2006.

[21] E. L. Madsen, M. A. Hobson, H. Shi, T. Varghese, and G. R. Frank, "Stability of heterogeneous elastography phantoms made from oil dispersions in aqueous gels," *Ultrasound Med. Biol.*, vol. 32, no. 2, pp. 261–270, 2006.

[22] K. Zell, J. Sperl, M. Vogel, R. Niessner, and C. Haisch, "Acoustical properties of selected tissue phantom materials for ultrasound imaging," *Phys. Med. Biol.*, vol. 52, pp. N475–N484, 2007.

[23] J. Fromageau, J.-L. Gennisson, C. Schmitt, R. L. Maurice, R. Mongrain, and G. Cloutier, "Estimation of polyvinyl alcohol cryogel mechanical properties with four ultrasound elastography methods and comparison with gold standard testings," *IEEE Trans. Ultrason., Ferroelect., Freq. Contr.*, vol. 54, no. 9, pp. 498–509, March 2007.

[24] U. Hamhaber, F. Grieshaber, J. Nagel, and U. Klose, "Comparison of quantitative shear wave mrelastography with mechanical compression tests," *Magn. Reson. Med.*, vol. 49, pp. 71–77, 2003.

[25] H. Mansy, J. Grahe, and R. Sandler, "Elastic properties of synthetic materials for soft tissue modeling," *Phys. Med. Biol.*, vol. 53, pp. 2115–2130, 2008.

[26] J. Fromageau, J.-L. Gennisson, C. Schmitt, R. L. Maurice, R. Mongrain, and G. Cloutier, "Estimation of polyvinyl alcohol cryogel mechanical properties with four ultrasound elastography methods and comparison with gold standard testing," *IEEE Trans. Ultrason., Ferroelect., Freq. Contr.*, vol. 54, no. 3, pp. 498–509, 2007.

[27] M. Doyley, J. Weaver, and K. Paulsen, "Measuring the mechanical properties of soft tissue over a wide frequency range by employing the principle of time temperature super-position," in *Proceedings of the Seventh International Conference on the Ultrasonic Measurement and Imaging of Tissue Elasticity*, Oct 2008, p. 75.

[28] S. Srinivasan, T. Krouskop, and J. Ophir, "A quantitative comparison of modulus images obtained using nanoindentation with strain elastograms," *Ultrasound Med. Biol.*, vol. 30, no. 7, pp. 899–918, 2004.

[29] D. Kalanovic, M. P. Ottensmeyer, J. Gross, G. Buess, and S. L. Dawson, "Independent testing of soft tissue viscoelasticity using indentation and rotary shear deformations," *Stud. Health Technol. Inform.*, vol. 94, pp. 37–43, 2003.

[30] V. Egorov, S. Tsyuryupa, S. Kanilo, M. Kogit, and A. Sarvazyan, "Soft tissue elastometer," *Med. Eng. Phys.*, vol. 30, pp. 206–212, 2008.

[31] A. Samani, J. Bishop, C. Luginbuhl, and D. B. Plewes, "Measuring the elastic modulus of ex vivo small tissue samples," *Phys. Med. Biol.*, vol. 48, pp. 2183–2198, 2003.

[32] H. Kolsky, *Stress Waves in Solids*. New York: Dover Publications, Inc., 1963.

[33] K. F. Graff, *Wave Motion in Elastic Solids*. Ely House, London: Oxford University Press, 1975.

[34] F. Lockett, *Non-linear Viscoelastic Solids*. London: Academic Press, 1972.

[35] W. Flugge, *Viscoelasticity*, 2nd ed. Berlin: Springer, 1975.

[36] S. Catheline, J. Gennisson, G. Delon, M. Fink, R. Sinkus, S. Abouelkaram, and J. Culiolic, "Measurement of viscoelastic properties of homogeneous soft solid using transient elastography: An inverse problem approach," *J. Acoust. Soc. Am.*, vol. 116, no. 6, pp. 3734–3741, Dec 2004.

[37] F. A. Duck, *Physical Properties of Tissue: A Comprehensive Reference Book*. Academic Press, 1990.

[38] T. Oliphant, A. Manduca, R. Ehman, and J. Greenleaf, "Complex-valued stiffness reconstruction by for magnetic resonance elastography by algebraic inversion of the differential equation," *Magn. Reson. Med.*, vol. 45, pp. 299–310, 2001.

[39] R. S. C. Cobbold, *Foundations of Biomedical Ultrasound*. Oxford University Press, 2006.

[40] H. Eskandari, S. E. Salcudean, and R. Rohling, "Viscoelastic parameter estimation based on spectral analysis," *IEEE Trans. Ultrason., Ferroelect., Freq. Contr.*, vol. 55, no. 7, pp. 1611–1625, 2008.

[41] R. Zahiri and S. Salcudean, "Motion estimation in ultrasound images using time-domain cross-correlation with prior estimates," *IEEE Trans. Biomed. Eng.*, vol. 53, no. 10, pp. 1990–2000, 2006.

APPENDIX

The measurement of the viscoelastic properties of the tissue phantoms at the frequencies considered in this article (between 50Hz to 100Hz) by conventional rheometry (force-displacement measurements) is a nontrivial problem. Here we elaborate on this issue.

In conventional compression based force-displacement rheometry, a block of test material with known dimensions $w \times l \times h$ is placed between two parallel plates (see Fig. 8). One of the plates is actuated and can move to compress the block. The force F needed to compress the material and the displacement of the moving plate d are measured. The stress and strain are found as,

$$\epsilon_{xx} = \frac{d}{h}, \tag{49}$$

$$\tau_{xx} = \frac{F}{w \times l}. \tag{50}$$

The elasticity (stiffness) of the material is found as,

$$E = \frac{\tau_{xx}}{\epsilon_{xx}}. \tag{51}$$

Conventional rheometry can also be used to study the behavior of the stiffness as a function of frequency. For this purpose the actuated plate of the device is excited by a time varying waveform, causing a time varying strain and a time varying stress. In this case, the stiffness would be

$$S(j\omega) = \frac{\mathcal{F}\{\tau_{xx}(t)\}}{\mathcal{F}\{\epsilon_{xx}(t)\}}. \tag{52}$$

where $\mathcal{F}()$ is the Fourier transform. The extension of static rheometry to a dynamic setting raises a number of very important issues which affect the measurement results. The first of these issues is the mounting of the force sensor. In the static case, the force sensor can be fitted between either of the plates and the rest of the device. In equilibrium the forces are different only by the weight of the test block and the weight of some parts of the force sensor. This difference can be measured and the device can be calibrated for this setting. In the dynamic case, however, there are significant issues related to each of the possible fittings.

Assume that the force sensor is fitted between the actuator of the device and the moving plate (Fig. 8). In this case the measured force by the sensor not only includes the applied force on the material block but also the inertial forces necessary to accelerate the plate and the mass of the block. The device needs to be calibrated, but the calibration is much more complicated than in the static setting. The inaccuracies involved in the measurements make this method very challenging to implement.

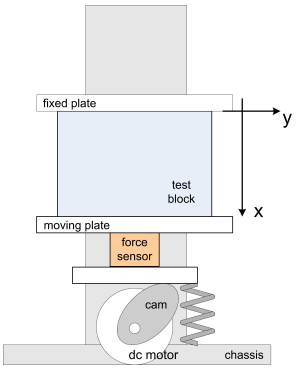

Fig. 8. Simple schematic of the rheometry device in a conventional rheometry configuration. In this configuration the force sensor measures the force on the moving plate and moves with it.

Another option is to fit the force sensor between the fixed plate and the chassis of the device (Fig. 9). Although in this case the measured force is the force applied to the block

to compress it from above, a second factor comes into play which complicates the problem. Due to the finite speed of propagation of longitudinal waves in the block, there would be a time delay (and hence a phase difference) between the measured force on the fixed end of the block and the force on the moving end of the block. The higher the frequency of the excitation, the larger the phase difference:

$$\phi(\omega) = \omega t = \omega \frac{h}{c_{\text{fin}}} \,. \tag{53}$$

If the velocity of the longitudinal waves c_{fin} were known, this formula could be used directly to compensate for the phase difference,

$$S(j\omega) = \frac{\mathcal{F}\{\tau_{xx}(t)\}}{\mathcal{F}\{\epsilon_{xx}(t)\}} \exp(j\phi(\omega)) \,, \tag{54}$$

but this velocity is itself a function of the stiffness (30):

$$c_{\text{fin}} = \sqrt{\frac{E}{\rho}} = \sqrt{\frac{\text{real}(S(j\omega))}{\rho}} \,. \tag{55}$$

This makes the measurement more challenging, but still feasible for low frequencies.

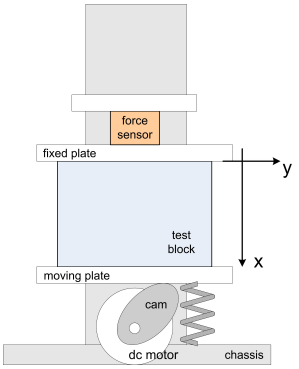

Fig. 9. Simple schematic of the rheometry device in a conventional rheometry configuration. In this configuration the force sensor measures the force on the static plate and does not move.

At higher frequencies, the problem becomes more severe. In fact equation (52) only applies to infinitesimal volumes of matter. Referring to Fig. 10, this equation states that if the only forces acting on the infinitesimal volume are perpendicular forces to the top and bottom surfaces, the strain and stress in the vertical direction are proportional, the proportionality factor being the Young's Modulus E. Whether this equation could be applied to a block of material depends on how similar the conditions are to the infinitesimal setting.

As far as the frequency is concerned, in the infinitesimal setting, the height of the block is always negligible with respect to the wave length of a propagating wave. This is not always true for a block. In other words, the block cannot always be considered as a *lumped element* with lumped mechanical properties equal to that of its infinitesimal elements. If the wave length is comparable to the height of the block, equation (52) would no longer be valid for the block.

One way to deal with the problem of the block not being a lumped element at higher frequencies is to reduce the height of the block, h. In other words, thin slabs could be used for

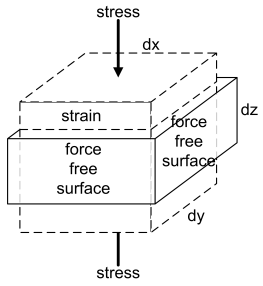

Fig. 10. The infinitesimal volume which is used in the definition of Elastic modulus.

rheometry measurements. But going back to the question of the similarity between the block and the infinitesimal settings, the boundary condition that "the only forces acting on the infinitesimal volume be perpendicular forces to the top and bottom surfaces" can never be achieved with the block; without any lubricant on the top and bottom plates of the device, the material would stick to the plates because of the friction and there would be tangential forces acting on the top and bottom surfaces of the block. The middle portion of the block, however, resembles the infinitesimal setting to a good extent. But reducing the block height h reduces the effective middle portion. Putting some lubricant helps but never removes the friction. It might be worth mentioning that this problem mainly appears for nearly incompressible material such as living tissue and tissue phantoms. These materials have a high tendency to expand laterally as they are compressed.

From this discussion, it follows that rheometry of soft tissue by conventional compression type force-displacement measurement at higher frequencies is not a trivial problem. In fact the proposed ultrasound based rheometry technique can be considered as a simple solution for this problem. Most commercially available rheometry devices use shear rheometry but their bandwidth is limited to 50Hz or bellow. Even with higher bandwidth systems, similar issues would exist with soft tissue since the test blocks would not be lumped at higher frequencies.

In this report we validated our estimated elasticity values with the values obtained from low frequency rheometry using the second configuration (Fig. 9). The relaxation times however could not be validated directly, except for the general trends.

Ali Baghani (S'05) received the B.Sc. degree in Electrical Engineering from Sharif University of Technology in 2004, and the M.Sc. degree in Electrical Engineering, Control Engineering Branch, from the University of Tehran in 2006. He was a visiting researcher at the Mita Labs, Tokyo Institute of Technology, under the YSEP program in 2001. He is currently a PhD candidate at the University of British Columbia. His previous research interests include mobile robots, nonholonomic constraints, nonlinear control, statistical pattern recognition, and Monte Carlo methods. His current research is focused on ultrasound elastography and ultrasound guided interventions.

Hani Eskandari (S'04, M'09) received the B.Sc. degree in Electrical Engineering in 2001 and the M.Sc. degree in Biomedical Engineering in 2003 from Sharif University of Technology, Iran and the Ph.D. degree in Electrical and Computer Engineering from the University of British Columbia in 2009. He is currently working as a research associate with the department of Electrical and Computer Engineering at the University of British Columbia. Dr. Eskandari's research interests include parameter estimation, inverse problems, biomedical signal processing and image analysis. His current research is focused on elastography, finite element modeling and parameter identification of soft tissues.

Septimiu (Tim) Salcudean (S'78, M'79, SM'03, F'05) received the B.Eng. and M.Eng. degrees from McGill University, Montreal, PQ, Canada, and the Ph.D. degree from the University of California, Berkeley, all in Electrical Engineering. From 1986 to 1989, he was a Research Staff Member in the robotics group at the IBM T.J. Watson Research Center, Yorktown Heights, NY. He then joined the Department of Electrical and Computer Engineering at the University of British Columbia, Vancouver, BC, Canada, where he is now a Professor and holds a Canada Research Chair and the C.A. Laszlo Professorship of Biomedical Engineering. He spent one year at ONERA-CERT (aerospace-controls laboratory) in Toulouse, France, in 19961997, where he held a Killam Research Fellowship, and six months, during 2005, in the medical robotics group (GMCAO) at CNRS in Grenoble, France. He has carried out research in haptics and teleoperation, medical robotics and tissue-needle interaction. His current interests include the imaging of mechanical properties of tissue and their use for image guided interventions. Prof. Salcudean has served as a Technical and Senior Editor of the IEEE TRANSACTIONS ON ROBOTICS AND AUTOMATION. He has been a co-organizer of several symposia on haptic interfaces. He is a Fellow of the Canadian Academy of Engineering.

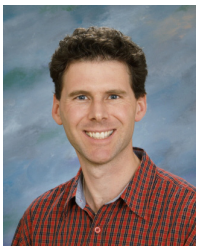

Robert Rohling (M'00) received the B.A.Sc. degree in engineering physics from the University of British Columbia (UBC), the M.Eng. degree in biomedical engineering from McGill University, and the Ph.D. degree in information engineering from the University of Cambridge. He worked as the project manager of 3D medical imaging at ALI Technologies from 19992000, before joining the University of British Columbia where he is now Associate Professor. He is a working member of DICOM on multidimensional interchange. He is a member of Precarn Inc. as part of a Network of Centres of Excellence. He is also the coordinator of the Biomedical Engineering Option and co-coordinator of the Mechatronics program at UBC. In 2002, he was awarded a New Opportunities Fund Award from the Canada Foundation for Innovation to establish a research laboratory called the Ultrasound Innovation Laboratory. His current research areas include adaptive ultrasound, 3D ultrasound, elastography and image-guided surgery.